Preprints (www.preprints.org) | NOT PEER-REVIEWED | Posted: 9 June 2021 doi:10.20944/preprints202106.0261.v1

Prediction of the direction of XFEM crack based on Von Mises around the crack-tip under mode-I.

Rehmat Bashir[1,2], He XUE[*1,] Muhammad Usman[2], Muneeb Irshad[2], Nasir Hayat[2]

[1] School of Mechanical Engineering, Xi'an University of Science and Technology, Xi'an 710054, China.

[2] Department of Mechanical Engineering, University of Engineering and Technology, Lahore-54890, Pakistan.

Abstract: The extended finite element method (XFEM) is now widely used in crack simulations and the direction of propagation of the XFEM crack in SS-304 has been quite interesting. This paper discusses the direction, $\boldsymbol{\theta}(\boldsymbol{+ve\ in\ anti-clockwise\ direction})$, of the XFEM crack (under mode-I) propagation based on the von Mises stress-field around the crack-tip for static loading under the light water reactors (LWRs) conditions. The Mises core region from the crack-tip is chosen for $\boldsymbol{\beta = 90^{o}}$, the angle between the load and the initial crack. Experimental data for LWRs'environment is obtained and the simulations have been carried out applying three different static loads and results for the direction of the crack are calculated by measuring the stress-field around the crack-tip. It has been found that the direction of the XFEM varies inversely as the stress-field around the crack tip is increased. The computational results have been compared with the numerical results based on the minimum strain energy density criterion[S-criterion].

Keywords: extended finite element method (XFEM); Von Mises; the direction of crack(θ); strain energy density criterion[S-criterion]; Mode-I

1. Introduction

Moës et al. [1, 2] proposed the extended finite element method (XFEM) method for crack growth simulations without re-meshing, and Farukh et al. [3] proved the capability of the XFEM predicting crack growth rate. The XFEM formulation is a powerful tool in numerical modeling and is now widely used for studying crack propagation under different loading and environmental conditions [4, 5]. With this method, mesh refinement is not required and results are closer to the actual values [6]. Unlike other cracks [7, 8], the XFEM cannot propagate at a constant rate i.e. the value of stress intensity factor (SIF) is changing at every instant of time rendering the XFEM crack direction an important field of research. Merely the presence of crack is not enough for the fracture analysis of the mechanical structures [9], the crack propagation and the path which would be adopted by the crack under the applied load is the key to reach the final destination of the damage. The damage consists of crack initiation, crack propagation, and failure [10]. The problem of the XFEM crack direction assuming the arbitrary stresses around the crack-tip was an interesting topic for the last few years. The direction of propagation of crack is quite necessary to be studied and known to locate the point of failure in the structure. The three basic modes of crack propagation; mode-I(opening), mode-II (in-plane shear/sliding), and mode-III (out-of-plane shear/tearing) are shown in Figure 1 [11]. The commonly used criterion, in the literature for the recent research, to predict the direction of the crack propagation are; the maximum tangential stress criterion(σ_0-Criterion) [12], principle of

*Correspondence: He XUE; Prof.at School of Mechanical Engineering ,Xi'an University of Science and Technology,Xi'an'China.xue_he@hotmail.com

Preprints (www.preprints.org) | NOT PEER-REVIEWED | Posted: 9 June 2021 doi:10.20944/preprints202106.0261.v1

local symmetry [13], the maximum energy release criterion(G-criterion) [14-16], and the maximum strain energy density criterion(S-criterion) [17, 18]. The typical aforementioned criteria rely on the Stress intensity factors (SIFs) which are determined using the auxiliary crack-tip fields [19].

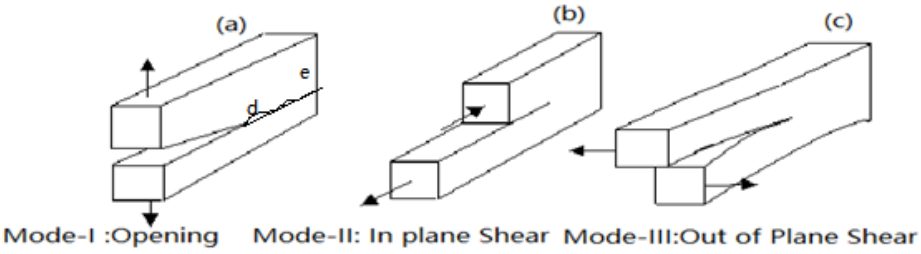

Figure 1. Modes of crack propagation.

Different authors have conducted researches based on simulation to predict the crack direction in single and mixed-mode [20-22], but a simple method has not yet been proposed to predict the direction of the crack. Apart from mixed mode, the direction of the crack in single-mode also varies concerning some arbitrary axis, see Figure 1(a) from the d-e region. In this paper, the prediction of the direction (angle, θ) of the XFEM under mode-I is discussed and the results are compared with the maximum strain energy density criterion(S-criterion). It is assumed that the specimen is the finite part of the Nuclear power Plants piping. Therefore, the mechanical properties of the specimen have been considered at the elevated temperature of 340 ^{o}C. A new and convenient technique, which is not available yet in the literature, about the prediction of the direction of the crack under mode-I has been introduced, which can be easily visualized by using Von Mises stress values around the crack-tip. The crack moves in the core region, not in straight line, but in zig-zag manners under mode-I. If the values of Von Mises stress around the crack-tip at different points are known, the tendency of the crack to deflect towards a point relative to other points can easily be predicted.

2. Materials and Methods

Austenitic Stainless steel is an important material used extensively in an aggressive environment like LWRs [23]. Low carbon stainless steel-304 is used in this research, which is an important type of stainless steel that has been used in many applications [24, 25]. Chemical and mechanical properties are shown in Tables 1. and 2. For plastic properties, the tensile true stress-strain curve is shown in Figure 2, for which the experimental data is obtained from the "Slow Strain Rate Stress Corrosion Testing Machine" available in Fracture Mechanics Lab of Xi'an University of Science and Technology, see Figure 3.

Table 1. Chemical composition of used stainless steel (wt.%).

STEEL	C	SI	MN	P	S	CR	N	NI
304	0.08	0.75	2.00	0.045	0.03	18-20	.10	8-10

Preprints (www.preprints.org) | NOT PEER-REVIEWED | Posted: 9 June 2021 doi:10.20944/preprints202106.0261.v1

Table 2. Elastic properties of the Stainless steel used.

MATERIAL	ELASTIC MODULUS	MAXIMUM PRINCIPAL STRESS	SHEAR MODULUS	POISSON'S RATIO	ELONGATION
STAINLESS STEEL	GPa	MPa	GPa	(v)	%
304	210	550	80	0.34	40

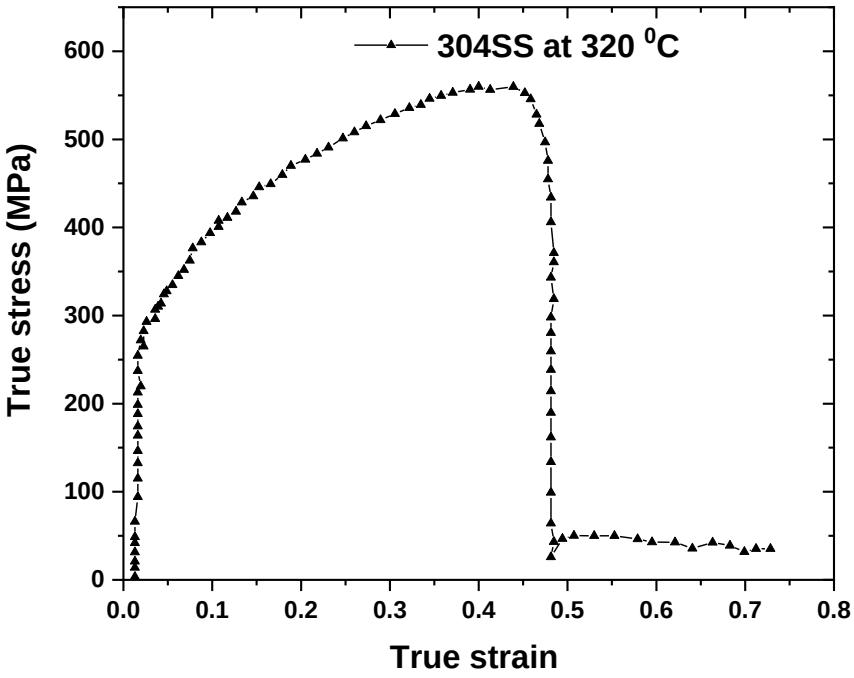

Figure 2. The tensile true stress-strain curve.

Figure 3. Slow Strain Rate Stress Corrosion Testing Machine.

Preprints (www.preprints.org) | NOT PEER-REVIEWED | Posted: 9 June 2021 doi:10.20944/preprints202106.0261.v1

Since real structures provide results closer to the practical values [26], therefore, a simple plate of 100mm ×50mm, having an embedded extended finite element method (XFEM) crack with 15mm is used as shown in Figure 4, along with the boundary conditions and loads. All the simulations have been performed in the ABAQUS 6.14 software following the instructions provided in the manual [27]. The uniformly distributed static-general loads of 200, 240, and 270MPa are applied separately on the top of the plate vertically which is explained in section 3.1. While the lower side is fixed, and the right side can elongate in the vertical direction only. The stress field is changed by changing the load and the step time and corresponding changes in the direction of propagation are estimated. Results are compared with the numerical values at the end.

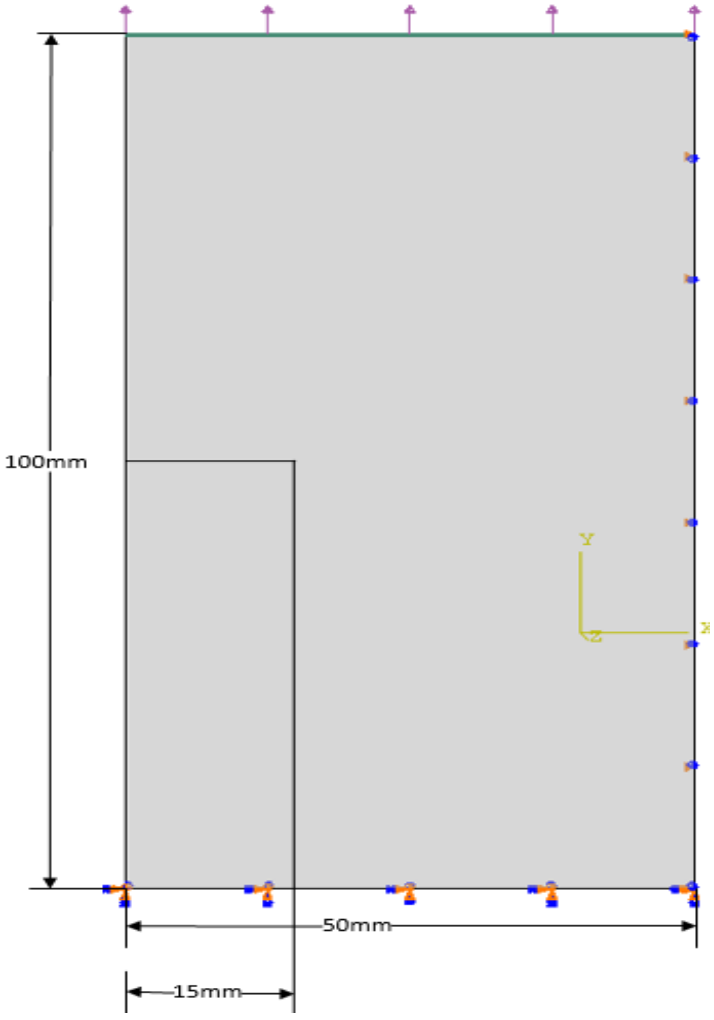

Figure 4. A schematic of the plate and loading scheme.

2.1. Application of Von Mises stress in S-criterion

The region ahead of the crack-tip is called the core region [28]. To obtain the von Mises plastic region(elastic-plastic region from crack-tip) [29] and the relation of crack direction with strain energy density, consider an elastic-plastic plate having an inclined crack at an angle,β, to the direction of a uniaxial load as shown in Figure 5.

Preprints (www.preprints.org) | NOT PEER-REVIEWED | Posted: 9 June 2021 doi:10.20944/preprints202106.0261.v1

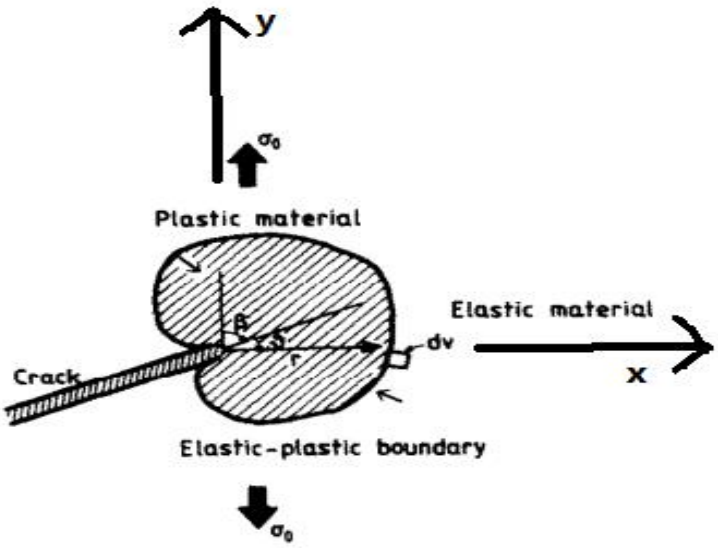

Figure 5. A schematic of the cracked plate showing different regions under uniaxial load.

The stresses around the crack-tip are given by Eq. (1);

$$\sigma_x = \frac{K_I}{\sqrt{2\pi r}}[\cos\frac{\theta}{2}-\frac{1}{2}\sin\theta\sin\frac{3\theta}{2} - R(2\sin\frac{\theta}{2}+\frac{1}{2}\sin\theta\cos\frac{3\theta}{2})] = \frac{K_I}{\sqrt{2\pi r}}f_x(\theta)\ ,$$

$$\sigma_y = \frac{K_I}{\sqrt{2\pi r}}[\cos\frac{\theta}{2}+\frac{1}{2}\sin\theta\sin\frac{3\theta}{2} + \frac{1}{2}R\sin\theta\cos\frac{3\theta}{2}] = \frac{K_I}{\sqrt{2\pi r}}f_x(\theta) = \frac{K_I}{\sqrt{2\pi r}}f_y(\theta)\ ,$$

$$\tau_{xy} = \frac{K_I}{\sqrt{2\pi r}}[\frac{1}{2}\sin\theta\cos\frac{3\theta}{2}+R(\cos\frac{\theta}{2} - \sin\theta\sin\frac{3\theta}{2})] = \frac{K_I}{\sqrt{2\pi r}}f_{xy}(\theta) \qquad (1)$$

Where r and θ are the polar coordinates and $R = \frac{\text{Stress intensity factor in mode}-II}{\text{stress intensity factor in mode}-I} = \frac{K_{II}}{K_I}$. The energy, T, per unit volume is

$$T = \frac{\partial W}{\partial V} = \frac{S(K_I,K_{II},\theta)}{r(\text{material constants})} \qquad (2)$$

Where S is named as strain energy density factor and is expressed as a function of Stress Intensity Factors and direction of crack and r is the Mises core region. Following the S-criterion, the extreme conditions for T are;

$$\frac{\partial T}{\partial\theta} = 0 \ \text{ Or } \ \frac{1}{r(\theta)}\frac{\partial S(\theta)}{\partial\theta} - \frac{S(\theta)}{r^2(\theta)}\frac{\partial r(\theta)}{\partial\theta} = 0 \qquad (3)$$

We assume that the equation of elastic-plastic boundaries is given in terms of distortion energy,T_D at .i.e $T_D = T_{D,0}$, where $T_{D,0}$ is the critical value of distortion energy and is given by

$$\sigma^2{}_1 + \sigma^2{}_2 - \sigma_1\sigma_2 = 0 \qquad (4)$$

By combining Eq. (1) and (4), after some algebra, we obtain;

$$r = \frac{(1+v)K_I{}^2}{6\pi ET_{D,0}}[f^2{}_1(\theta) + f^2{}_2(\theta) - f_1(\theta)f_2(\theta)] \qquad (5)$$

Preprints (www.preprints.org) | NOT PEER-REVIEWED | Posted: 9 June 2021 doi:10.20944/preprints202106.0261.v1

Where

$$f_{1,2}(\theta) = \frac{1}{2}\left[f_x(\theta) + f_y(\theta)\right] \pm \frac{1}{2}[\{f_x(\theta) - f_y(\theta)\}^2 + 4f^2{}_{XY}(\theta)]^2 \qquad (6)$$

Let $A = \frac{(1+v)K_I{}^2}{6\pi E T_{D,0}}$ and $F(\theta) = [f^2{}_1(\theta) + f^2{}_2(\theta) - f_1(\theta)f_2(\theta)]$ then Eq.(5) can be written as

$$F(\theta) = \frac{r}{A} \qquad (7)$$

Where, r, Mises core region can be calculated by using Eq. (5), see Figure 6, and it depends upon the applied load direction as well.

It is obvious from Figure 6, for an angle $\beta = 90^o$ (angle between the load and the initial direction of the crack), the Mises core region is uniformly maximum while in the case of $\beta = 60^o, the$ core region is slightly larger on some points but not uniform.

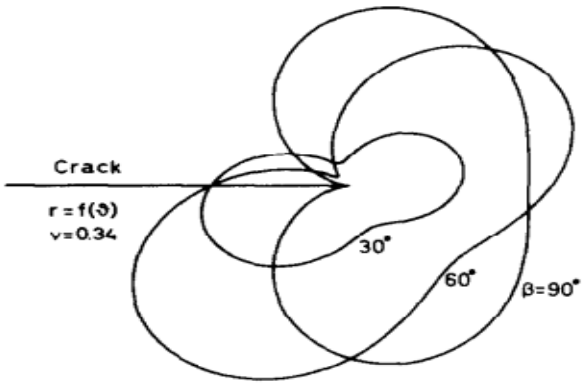

Figure 6. The variations in Mises elastic boundary around the crack-tip, for β = 30^0, 60^0 and 90^0.

2.2. Finite element model and Crack growth simulations

A typical 4-node finite element mesh model with 12093 elements is shown in Figure 7a(Global Mesh) where X-coordinate is parallel to the direction of crack and Y-coordinate is normal to the direction of crack. A small subset in circular form is generated around the crack-tip to visualize the crack growth rate clearly, see Figure 7b(Local Mesh).

Preprints (www.preprints.org) | NOT PEER-REVIEWED | Posted: 9 June 2021 doi:10.20944/preprints202106.0261.v1

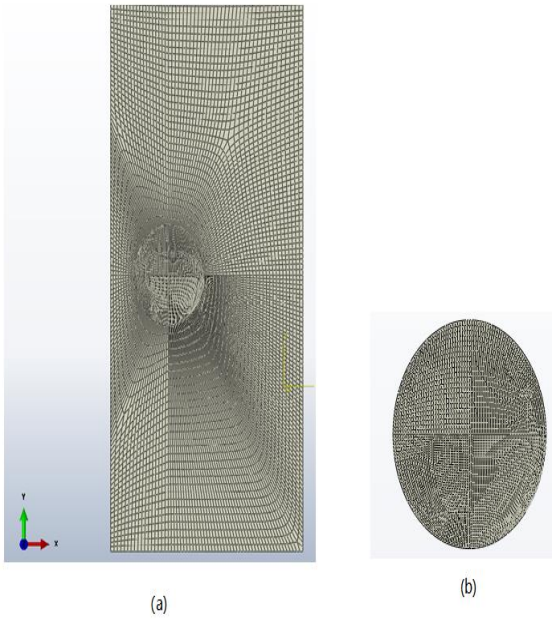

Figure 7. (a) Global mesh (b) local mesh.

The maximum principal stress criterion is used which is represented as follow.

$$f = \{\frac{\sigma_{max}}{\sigma^0_{max}}\} \quad (8)$$

Where σ^0_{max}represents the maximum allowable principal stress and the damage starts when the ratio becomes unity [30]. The damage evolution technique based on power law has been used to simulate crack propagation. In the case of Static loading, the step time is 1sec with a 0.001 increment size.

3. Results and Discussions

It can be seen from Figure 8, at constant step-time=1000 (constant stress distribution refinement), the starting and ending values of the stresses at minimum load are minimum and those at maximum load are maximum. Variations can be seen from the initial crack-tip(0mm) to onwards.

It is obvious from Figure 9, at step time=100, the difference between starting and ending values of the stress is too high while at step-time=1000 the difference between starting and ending values of the stress is not too high. This is because the increase in the step-size increases the stress distribution refinement.

Figure 8 shows, as the applied load increases, while keeping the step-time constant, the values of the Von Mises stress field around the crack-tip increase concerning the distance from the crack. And Figure 9 shows, as the step-time is increased, while keeping the applied load constant, the values of the stress field around the crack-tip concerning the distance from the crack also increases. Hence the values of the stress field around the crack-tip may be increased either by increasing the step-time at constant applied load or applied load at constant step-time.

Preprints (www.preprints.org) | NOT PEER-REVIEWED | Posted: 9 June 2021 doi:10.20944/preprints202106.0261.v1

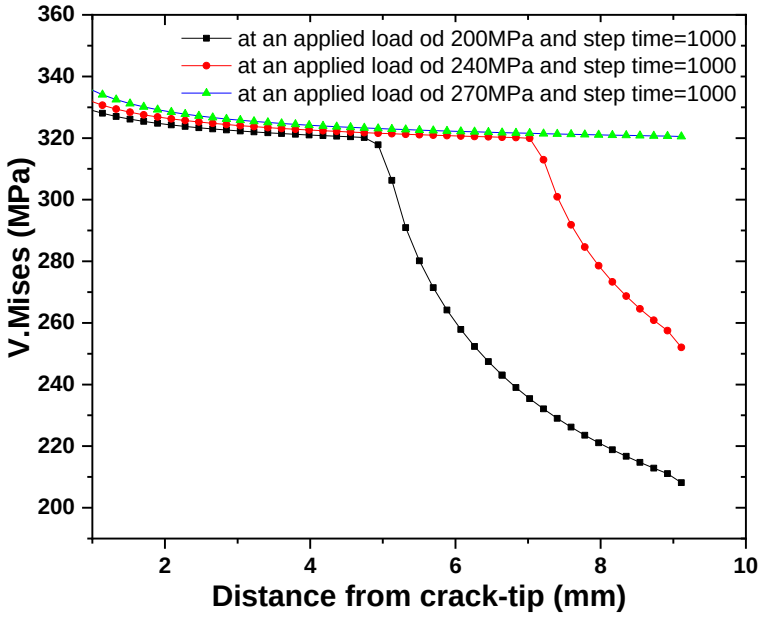

Figure 8. Variations in Von Mises stress at various applied loads.

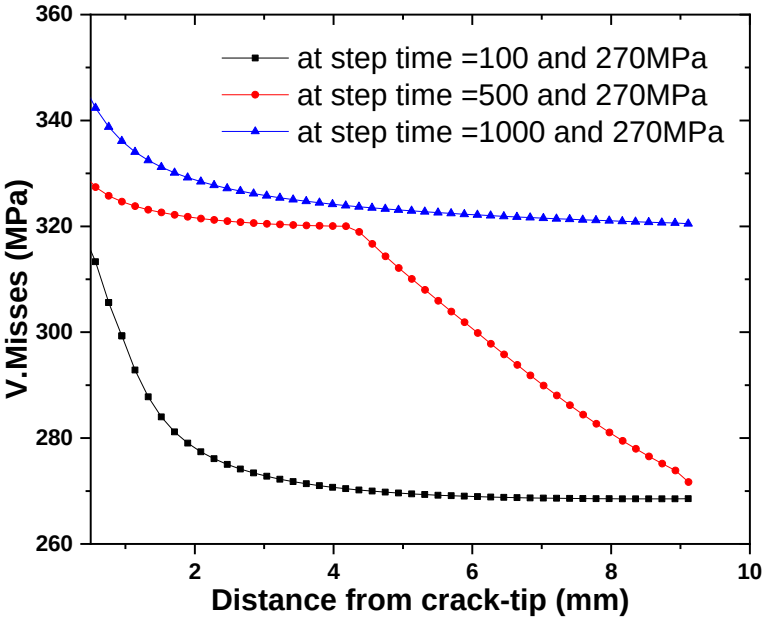

Figure 9. Variations in Von Mises stress at different step-time.

3.1. Computational results

Figures 10 and 11 represent the relationship between the direction of crack propagation and Von Mises at three different applied static loads. The stress field is increased by increasing the

Preprints (www.preprints.org) | NOT PEER-REVIEWED | Posted: 9 June 2021 doi:10.20944/preprints202106.0261.v1

step-time and the process is repeated at three different applied loads to validate the decreasing trend of angle w.r.t. an increase in the stress field around the crack-tip.

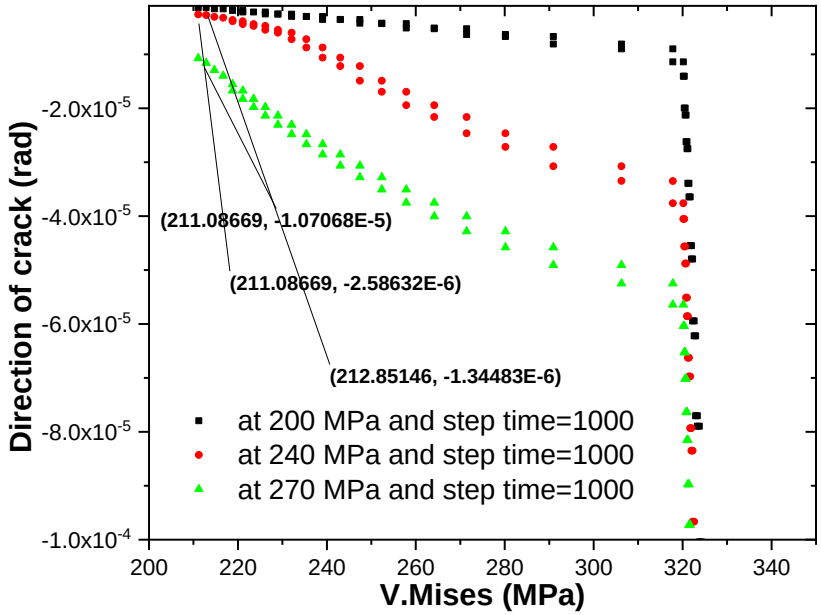

Figure 10. Effect of variations in applied on **the** direction of crack propagation at step-time=1000.

It is clear from these two figures, as the values of the stress field increases, the crack propagation direction tends to be small. The computational results have been calculated directly from the ABAQUS by using Eq. (9)

$$\vartheta(\text{radians}) = \lim_{\Delta a \to 0} \frac{\Delta u_y}{\Delta a} \qquad (9)$$

Where ϑ is the angle with the positive x-axis(axis parallel to the propagation direction) and it is measured in radians and $\lim_{\Delta a \to 0} \frac{\Delta u_y}{\Delta a}$ is the ratio of the vertical displacement to the horizontal true distance.

Preprints (www.preprints.org) | NOT PEER-REVIEWED | Posted: 9 June 2021 doi:10.20944/preprints202106.0261.v1

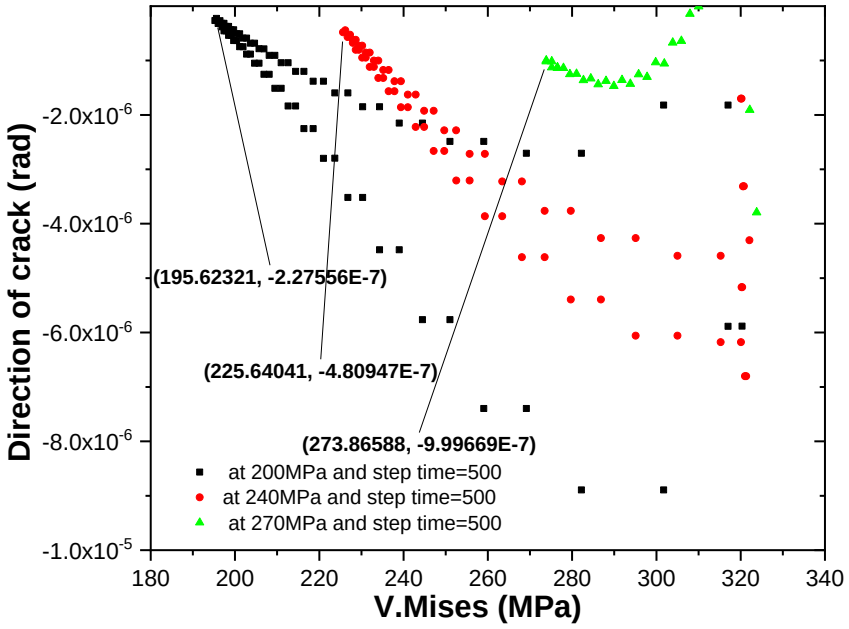

Figure 11. Effect variations in applied load on the direction of crack propagation at step time=500.

3.2. Comparison with numerical results and validation

Figure 12 shows the comparison of the computational and numerical results. The numerical results are calculated by using Eq. (7).r is measured by taking the Mises core region directly from ABAQUS as shown in Figure 6, for $\beta = 90^{o}$and SIF for pure mode-I in factor A is measured by using the following process: from Eq. (2) it is clear that S is the function of SIFs and angle which can be described as

$$S = a_{11}K^2_I + 2a_{12}K_IK_{II} + a_{22}K^2_{II} \quad (10)$$

Where

$$a_{11} = \frac{1}{16\pi G}(k - \cos\theta)(1 + \cos\theta),$$

$$a_{12} = \frac{1}{16\pi G}\sin\theta\{(2\cos\theta) - (k - 1)\}, \text{ and}$$

$$a_{22} = \frac{1}{16\pi G}\{(k + 1)(1 - \cos\theta) + (1 + \cos\theta)(3\cos\theta - 1)\} \quad (11)$$

Where $k=\frac{3-v}{1+v}$ for plane stress and $3 - 4v$ for plane strain. From Eq. (10) and (11), for pure mode-I.

$$K_I = \left[\frac{16\pi GS}{(k-\cos\theta)(1+\cos\theta)}\right]^{1/2} \quad (12)$$

Using Eq. (12) in terms of angle is used into Eq. (7), and the results are computed, see Figure 12. Because the values of stress intensity factors in the case of XFEM are changing at every instant of time, so they cannot be computed by traditional formulas and here the strain energy density values are calculated from ABAQUS.

Preprints (www.preprints.org) | NOT PEER-REVIEWED | Posted: 9 June 2021 doi:10.20944/preprints202106.0261.v1

Figure 13 shows the validity of the work according to minimum strain energy density(S-criterion) which states that the direction of crack growth is towards the region with a minimum value of strain energy [31].

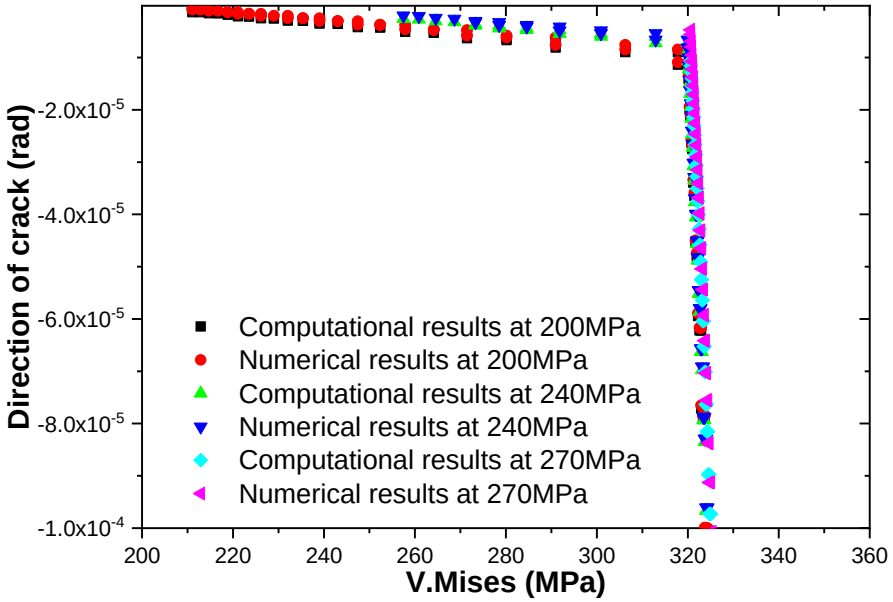

Figure 12. Comparison of computational and theoretical results.

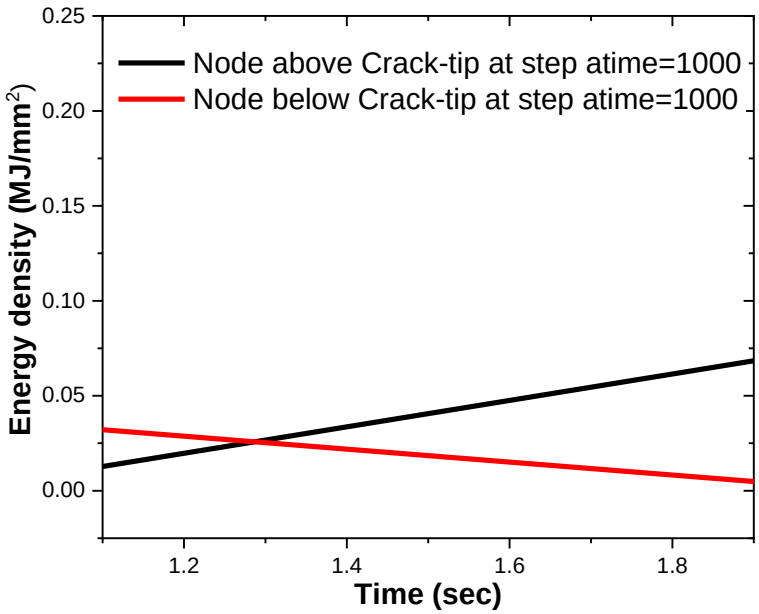

Figure 13.The validity of the S-criterion.

Preprints (www.preprints.org) | NOT PEER-REVIEWED | Posted: 9 June 2021 doi:10.20944/preprints202106.0261.v1

4. Conclusions

A new technique to visualize /predict the direction under mode-I based on Von Mises stress has been introduced which is helpful to predict the direction directly from simulation results rather than formulating or calculating the results of the direction of the crack based on direction predicting criteria.

The XFEM is now being used widely in crack simulations and is well known for taking its path even in a single direction unlike debonding crack and this technique helps to judge the direction of the crack in a single mode (along one direction) based on the visual observations (von Mises stress values) directly from the software being used for simulations [The relationship between von Mises stress (directly from the ABAQUS) and the direction of the crack]. The following conclusions can be drawn.

With an increase in the applied load, slight variations were observed in the immediate vicinity of the crack-tip for the values of the Von Mises stresses around the crack-tip. With an increase in the distance from the crack-tip, a different pattern was observed for maximum load in contrast to the minimum load wherein Von. Mises stresses drop sharply at lower load for a relatively larger distance from the crack-tip.

With the increase of the step-time at constant loading, the values of the Von Mises around the crack-tip increases. Relatively large variations in the values of Von Mises stresses are observed and the pattern for the drop of Von Mises at a relatively larger distance from the initial crack-tip is the same as it was observed at constant step-time with different applied loads.

As the values of Von Mises stress increase, the values of the direction of propagation of XFEM crack decrease but the absolute values increase which satisfies the minimum strain energy criterion theoretically as well i.e., crack tends to move towards the decreasing region of strain energy.

Acknowledgments: Our work was financially supported by the National Natural Science Foundation of China (52075434) and the Natural Science Foundation of Shaanxi Province (2021JM-389, 2021KW-36).

Conflicts of Interest: The authors declare that there is no conflict of interest.

References

1. Moes, N.; Dolbow,J.; Belytschko,T. *Elastic crack growth in finite elements without remeshing. Int J Numer Methods Eng* **1999**, 46, 131-150.
2. Sukumar, N.; et al. *Extended finite element method for three-dimensional crack modelling. Int J Numer Methods Eng* **2000**, 48(11), 1549-1570.
3. Farukh, F.; et al. Fatigue crack growth in a nickel-based superalloy at elevated temperature-experimental studies, viscoplasticity modelling and XFEM predictions. *Mech Adv Mater Mod Process* **2015**, 1(1), 1-13.
4. Zhuang, Z.; et al. *Extended Finite Element Method: Tsinghua University Press Computational Mechanics Series* **2014**, DOI:10.1016/C2012-0-01326-9.

5. Zhao, J.; et al. *A method for modeling the transition of weak discontinuities to strong discontinuities: from interfaces to cracks. Int J Numer Methods Eng* **2016,** 105(11), 834-854.
6. Yau, J.; Wang,S.; Corten, H. A mixed-mode crack analysis of isotropic solids using conservation laws of elasticity. *J Appl Mech Trans ASME* **1980,** DOI:10.1115/1.3153665.
7. Xue, H.; et al. The effect of a single tensile overload on stress corrosion cracking growth of stainless steel in a light water reactor environment. *Nucl. Eng. Des*. **2011,** 241(3), 731-738.
8. Lu, Z.; et al. *Locally Delaminating Stress Corrosion Cracking Growth of Strain-Hardened Austenitic Alloys in Hydrogenated High Temperature Water Environments*. *Am Soc Mech Eng Press Vessel Pip Div PVP* **2010**, DOI:10.1115/PVP2009-77622.
9. Bergara, A.; et al. *Fatigue crack propagation in complex stress fields: Experiments and numerical simulations using the Extended Finite Element Method (XFEM). Int J Fatigue* **2017**, 103, 112-121.
10. Giner, E.; et al. *An Abaqus implementation of the extended finite element method. Eng Fract Mech* **2009**, 76(3), 347-368.
11. Sun, C.T.; Jin, Z. Chapter 1 – Introduction. *Fract. Mech*. **2012**, DOI:10.1016/B978-0-12-385001-0.00001-8.
12. Erdogan, F.; Sih, G. *On the crack extension in plates under plane loading and transverse shear. J Fluids Eng Trans ASME* **1963**, DOI:10.1115/1.3656897.
13. Gol'dstein, R.V.; Salganik, R.L. *Brittle fracture of solids with arbitrary cracks. Int J Fract* **1974**, 10(4), 507-523.
14. Palaniswamy, K.; Knauss,W. *Propagation of a crack under general, in-plane tension. Int J Fract Mech* **1972**, **8**(1), 114-117.
15. Hussain, M.A.; Pu, S.L.; Underwood, J. *Strain Energy Release Rate for a Crack Under Combined Mode I and Mode II. Natl Symp Fract Mech* **2009,** 2, 2–27.
16. Karihaloo, B.; Keer, L.; Nemat-Nasser, S. *Crack kinking under nonsymmetric loading. Eng Fract Mech* **1980**, 13(4), 879-888.
17. Hayashi, K.; Nemat-Nasser, S. *Energy-release rate and crack kinking under combined loading. J Appl Mech Trans ASME* **1981**, DOI:10.1115/1.3157666.
18. Sih, G.C. *Some basic problems in fracture mechanics and new concepts. Eng Fract Mech* **1973**, 5(2), 365-377.
19. Williams, M. On the stress distribution at the base of a stationary crack. *J Appl Mech* **1956,** DOI:10.1093/bja/54.11.1237.
20. Frank, F.; Stroh, A. *On the theory of kinking.* Proc. Phys. Soc. Sect. B **1952**, 65(10), 811.
21. Nuismer, R. *An energy release rate criterion for mixed mode fracture. Int J Fract* **1975**, 11(2), 245-250.
22. Shu, B.; et al. *A qualitative prediction method of new crack-initiation direction during hydraulic fracturing of pre-cracks based on hyperbolic failure envelope. Appl Energy* **2019**, 248, 185-195.
23. Dahlberg, M.; Bremberg, D. *Fatigue margins for austenitic stainless steels in ASME Boiler and pressure vessel code–a literature study. Publ Swedish Radiat Saf Auth* **2012**.
24. Hu, X.; et al. *Hydrogen permeation in FeCrAl alloys for LWR cladding application.* J Nucl Mater **2015**, 461, 282–91.

25. Szklarska-Smialowska, S.; Cragnolino, G. *Stress corrosion cracking of sensitized type 304 stainless steel in oxygenated pure water at elevated temperatures. Corrosion* **1980**, 36(12), 653-665.
26. Bashir, R.; et al. *Interaction of Cyclic Loading (Low-Cyclic Fatigue) with Stress Corrosion Cracking (SCC) Growth Rate. ADV MATER SCI ENG*, **2020**.
27. Fish, J.; Belytschko, T. Commercial Finite Element Program ABAQUS Tutorials. *A First Course Finite Elem.* **2007,** DOI:10.1002/9780470510858.ch11.
28. Bashir, R.; et al. *Effect of XFEM mesh density (mesh size) on stress intensity factors (K), strain gradient (dεdr) and stress corrosion cracking (SCC) growth rate. Structures* **2020**, 25, 593-602.
29. Theocaris, P.; Andrianopoulos, N. *The Mises elastic-plastic boundary as the core region in fracture criteria. Eng Fract Mech* **1982**,16, 425–32.
30. Abaqus, V. 6.14 Documentation. *Dassault Systemes Simulia Corporation* **2014**, 651, 6.2.
31. Aliabadi, M.H. *3.02 - Boundary Element Methods in Linear Elastic Fracture Mechanics. Compr Struct Integr* **2007**, 3, 89–125.